Nuclear Materials and Energy 36 (2023) 101473

Contents lists available at ScienceDirect

Nuclear Materials and Energy

journal homepage: www.elsevier.com/locate/nme

Measurement of thermal expansion anisotropy in $Be_{12}Ti$ and $Be_{12}V$

Keisuke Mukai [a,*], Jae-Hwan Kim [b], Masaru Nakamichi [b]

[a] Institute of Advanced Energy, Kyoto University, Gokasho, Uji, Kyoto 611-0011, Japan
[b] Fusion Energy Directorate, National Institutes for Quantum Science and Technology, 2-166 Omotedate, Obuchi, Rokkasho, Aomori, 039-3212, Japan

ARTICLE INFO

Keywords:
Nuclear fusion
Neutron multiplier
Anisotropic thermal expansion
Beryllium intermetallics

ABSTRACT

$Be_{12}Ti$ and $Be_{12}V$ are promising candidates for neutron multipliers in solid breeding blankets, which is used in a bulk form to achieve the fuel tritium self-sufficiency. Previously, significant anisotropic thermal expansions were predicted for $Be_{12}Ti$ and $Be_{12}V$ along different crystallographic axes using density functional theory (DFT) calculations. Nevertheless, empirical confirmation through experimental data on thermal expansion anisotropy remains lacking. In this study, the thermal expansion behaviors of these materials were experimentally investigated by using high-temperature X-ray diffraction. Diffraction data were collected temperatures up to 873 K under vacuum condition, and structural refinement was carried out by Le Bail analysis using a partial structure. The results demonstrate that these materials exhibit moderate anisotropic expansion along the *c*-axis direction, contrary to previous prediction for $Be_{12}Ti$. The average thermal expansion coefficients were compared with those of ceramic breeder pebble beds and structural steel material to discuss thermo-mechanical compatibility in a breeding blanket.

Introduction

In the breeding blanket of a fusion reactor, a neutron multiplier is used for a self-sufficient production of fuel tritium. Be intermetallics (i.e., beryllides) have been developed as advanced neutron multiplier. An advantage of beryllides is their oxidation resistance at elevated temperatures, which can significantly reduce hydrogen production by the reaction with water vapor in a loss-of-coolant accident [1–3]. Experimental investigations have shown that $Be_{12}Ti$ and $Be_{12}V$ exhibit superior irradiation resistance and tritium release properties compared with conventional pure Be neutron multiplier [4–9]. Computational assessments have been extensively performed for Be-rich beryllides to investigate their electron structures [10,11], H and He retention [4,12,13], tritium diffusion [14], and defect formation [15,16]. While neutron multipliers were originally planned for use in the pebble form in blanket, current DEMO blanket design proposes loading it in block form to increase the tritium breeding ratio and reduce the fabrication cost. In the water-cooled solid breeding blanket for JA-DEMO, the beryllide block contains Li_2TiO_3 ceramic breeder pebbles [17], while hexagonal beryllide block is employed in the European helium cooled pebble bed (HCPB) blanket with Li_4SiO_4-Li_2TiO_3 bi-phasic pebbles [18,19].

$Be_{12}Ti$ and $Be_{12}V$ have tetragonal crystal structure with the unit cell parameters $a = b \neq c$ and $\alpha = \beta = \gamma = 90°$. The thermal expansion coefficient α is a fundamental and crucial parameter for blanket design because it is operated at elevated temperatures. A previous study has computationally investigated the thermal expansion coefficients α, the heat capacity, and thermal conductivity of $Be_{12}Ti$ and $Be_{12}V$ using density functional theory (DFT) in combination with the quasi-harmonic approximation [11]. It is predicted that $Be_{12}Ti$ and $Be_{12}V$ have significant anisotropic thermal expansion characteristics towards opposite directions while having the same crystal symmetry; $Be_{12}Ti$ has a significantly high anisotropic thermal expansion along the *a*- and *b*-axes ($\alpha_a/\alpha_c \sim 2.9$ at 873 K), while $Be_{12}V$ preferentially expands along the *c* axis direction ($\alpha_a/\alpha_c \sim 0.4$ at 873 K). These magnitudes of anisotropy were at least two times larger than that of hexagonal close-packed Be ($\alpha_a/\alpha_c = 0.8$ at 873 K [20]). Such thermal expansion behavior requires an experimental validation because significant anisotropy could induce thermal stress when operating at high temperatures. However, no experimental data on anisotropy in thermal expansion have been reported to date, an the only available data pertains to the average thermal expansion coefficient [21]. Herein, thermal expansion anisotropies of $Be_{12}Ti$ and $Be_{12}V$ were investigated using high-temperature X-ray diffraction (XRD). The diffraction patterns from polycrystal beryllide specimens were measured at high temperatures up to 873 K and analyzed by Le Bail method using a partial structure. The thermal expansion data obtained were compared with the computational results

* Corresponding author.
E-mail address: k-mukai@iae.kyoto-u.ac.jp (K. Mukai).

https://doi.org/10.1016/j.nme.2023.101473
Received 24 May 2023; Received in revised form 30 June 2023; Accepted 6 July 2023
Available online 7 July 2023

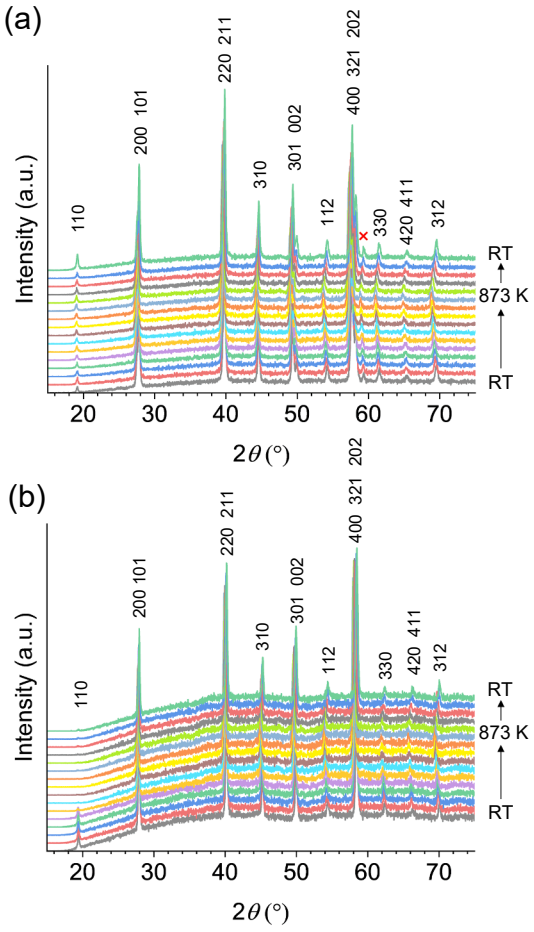

Fig. 1. High temperature X-ray diffraction patterns of the (a) $Be_{12}Ti$ and (b) $Be_{12}V$ samples measured from room temperature (RT) to 873 K. Red cross in panel (a) represents impurity peak.

and those of other blanket materials, including reduced activation ferritic martensitic (RAFM) steel and ceramic breeder pebble beds.

Methods

$Be_{12}Ti$ and $Be_{12}V$ specimens were prepared by plasma-sintering method [3]. The starting materials were Be (Materion Brush, USA, purity: 99.4 wt%), Ti (>99.9 wt%), and V (>99 wt%) powders. The powders were mixed at an atomic ratio of 92.3% (Be) and 7.7% (Ti or V). The powder mixtures were cold-pressed and then plasma-sintered at 1050 °C for 20 min at 50 MPa. The sintered specimens were cut into plates with thickness of 1.2 mm.

High temperature XRD was performed with RINT TTR-III diffractometer (Rigaku) using Co–Kα radiation in a 2θ range from 15 to 75° at intervals of 0.02°. To avoid possible scale formation, hydrogen generation, or powder scattering in high temperature XRD, the experiments were conducted in a vacuum condition at relatively low temperatures (i.e. maximum 873 K). The measurements were performed by parallel beam mode. XRD patterns were collected at room temperature (RT), 423, 473, 523, 573, 623, 673, 723, 773, 823, and 873 K by heating up at a heating rate of 10 K/min. During cooling, the data were collected at 773, 673, 573, 473, and RT at a cooling rate of 50 K/min. Temperature of the sample was monitored using a thermo-couple attached to the sample holder. The measurements were performed under vacuum conditions, in which the pressure was maintained at <1 Pa. Le Bail analysis using the partial structure was performed with the RIETAN-FP software [22]. Thermal expansion coefficient along *a* and *c* axis are calculated as

Table 1
Results of Le Bail analysis on the X-ray diffraction data of (a) $Be_{12}Ti$ and (b) $Be_{12}V$ at 300–873 K. The equations are linear functions with temperature *T* (K) obtained from the data measured during heating.

T (K)	R_{wp}	R_B	*S*	*a* (Å)	*c* (Å)	*V* (Å^3)
(a)						
303	8.86	4.70	1.18	7.3763(6)	4.2003(3)	228.54(3)
423	8.93	4.42	1.19	7.3846(3)	4.2077(2)	229.46(2)
473	8.99	4.85	1.19	7.3889(6)	4.2109(3)	229.89(3)
523	9.16	4.42	1.21	7.3949(3)	4.2156(2)	230.53(2)
573	9.11	4.04	1.20	7.3995(3)	4.2196(2)	231.03(2)
623	9.24	4.18	1.22	7.4059(3)	4.2238(2)	231.67(2)
673	9.21	0.28	1.21	7.4099(5)	4.2275(3)	232.11(3)
723	8.83	4.40	1.16	7.4146(6)	4.2312(3)	232.61(3)
773	9.12	4.33	1.20	7.4179(5)	4.2345(3)	233.00(3)
823	8.95	3.76	1.17	7.4256(5)	4.2401(3)	233.80(3)
873	8.98	4.01	1.18	7.4309(3)	4.2444(2)	234.37(2)
773	8.99	4.10	1.18	7.4197(3)	4.2357(2)	233.18(2)
673	9.31	4.45	1.23	7.4101(3)	4.2273(2)	232.12(2)
573	8.77	4.28	1.16	7.3976(3)	4.2180(2)	231.83(2)
473	9.26	0.42	1.22	7.3877(3)	4.2098(2)	229.76(1)
300	8.51	3.41	1.20	7.3732(4)	4.1991(2)	228.28(2)

Temperature dependency of the lattice parameters: $a = b = 7.344 + 9.754 \times 10^{-5} \times T$, $c = 4.175 + 7.820 \times 10^{-5} \times T$, $V = 225.1 + 1.038 \times 10^{-2} \times T$

T (K)	R_{wp}	R_B	*S*	*a* (Å)	*c* (Å)	*V* (Å^3)
(b)						
301	5.89	4.80	1.29	7.3383(4)	4.2301(3)	227.79(3)
423	5.85	5.29	1.27	7.3498(5)	4.2385(4)	228.96(3)
473	5.63	6.20	1.21	7.3558(4)	4.2432(3)	229.59(2)
523	5.86	5.42	1.26	7.3619(4)	4.2465(3)	230.15(2)
573	5.59	5.51	1.20	7.3676(3)	4.2501(3)	230.70(2)
623	5.73	6.52	1.20	7.3720(4)	4.2534(3)	231.16(2)
673	6.05	6.94	1.27	7.3816(4)	4.2597(3)	232.10(3)
723	5.85	6.88	1.23	7.3869(4)	4.2629(2)	232.61(2)
773	5.76	6.58	1.21	7.3920(5)	4.2684(2)	233.23(2)
823	5.97	6.31	1.26	7.3952(4)	4.2703(2)	233.54(2)
873	5.74	5.85	1.22	7.3973(6)	4.2731(3)	233.82(3)
773	5.97	6.39	1.26	7.3904(5)	4.2682(3)	233.12(3)
673	5.93	6.23	1.25	7.3803(4)	4.2595(2)	232.05(2)
573	5.82	6.74	1.22	7.3678(6)	4.2500(3)	230.71(3)
473	5.87	7.38	1.23	7.3536(6)	4.2392(4)	229.24(4)
300	5.86	5.79	1.23	7.3380(5)	4.2293(4)	227.73(4)

Temperature dependency of the lattice parameters: $a = b = 7.304 + 1.109 \times 10^{-4} \times T$, $c = 4.206 + 7.847 \times 10^{-5} \times T$, $V = 224.3 + 1.121 \times 10^{-2} \times T$

$\alpha_a = da/dT/a_0$ and $\alpha_c = dc/dT/c_0$ where a_0 and c_0 are the lattice parameters at RT. The average thermal expansion coefficient is given by $\alpha_V = d(V)^{1/3}/dT/(V_0)^{1/3}$ where V_0 is the unit cell volume at RT.

Results and discussion

Fig. 1 shows the diffraction patterns of the $Be_{12}Ti$ and $Be_{12}V$ specimens during heating and cooling measured at temperatures ranging from RT to 873 K. The peaks were indexed to the tetragonal structures of $Be_{12}Ti$ and $Be_{12}V$ with the space group of $I4/mmm$. The weak peak at ~59.3° in the $Be_{12}Ti$ specimen was unindexed, which could be an impurity phase. The peak intensity at 2 θ = 19.4° in the $Be_{12}V$ specimen became weak above 350 °C and remained constant at the background-level during the cooling process. Although the peak position corresponds to the diffraction from the (1 1 0) plane of $Be_{12}V$, the peak below 350 °C could correspond to another Be–V intermetallic phase that decomposed during heating. The diffraction data in the 2 θ range from 20 to 75° were used in the Le Bail analysis, in which the data from 58.7° to 59.5° were excluded for $Be_{12}Ti$ to exclude the unindexed minor peak.

The reliability factors and refined lattice parameters of the Le Bail analysis with the partial structure are summarized in Table 1. Fig. 2 shows the results of the analysis on the diffraction data at 873 K. The observed diffraction patterns were indexed with the $I4/mmm$ structure

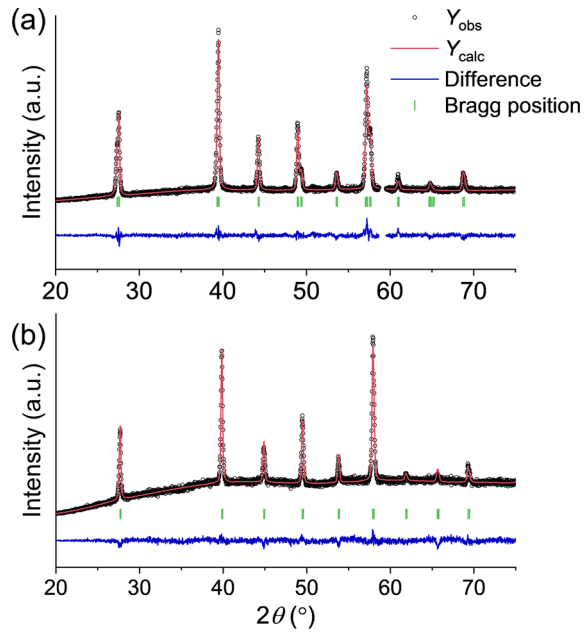

Fig. 2. Le Bail analysis of the diffraction patterns of the (a) $Be_{12}Ti$ and (b) $Be_{12}V$ specimens at 873 K. The black circle, red solid line, blue solid line, and green tick marks denote the observed intensity Y_{obs}, calculated intensity Y_{calc}, the difference $Y_{obs} - Y_{calc}$, and calculated Bragg peak positions, respectively.

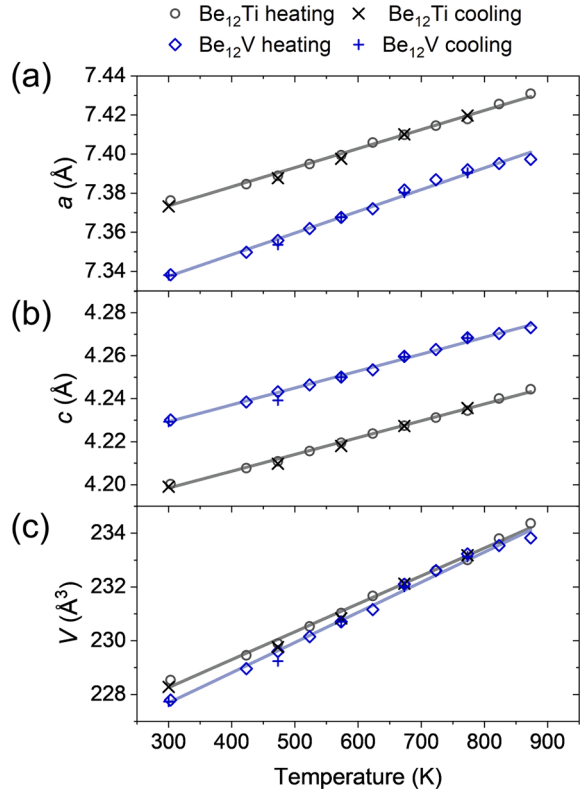

Fig. 3. Temperature dependence of the lattice parameters (a) a, (b) c, and (c) lattice volume V with line fittings for the data obtained during heating. The equations of line fittings are shown in Table 1.

and fit well to the calculated pattern after the refinements. No new peak arising from phase transformation or surface oxidation was observed from the measured data. The reliability factors R_{wp}, R_B, and S correspond to the weighted profile R-factor, Bragg R-factor, and square root

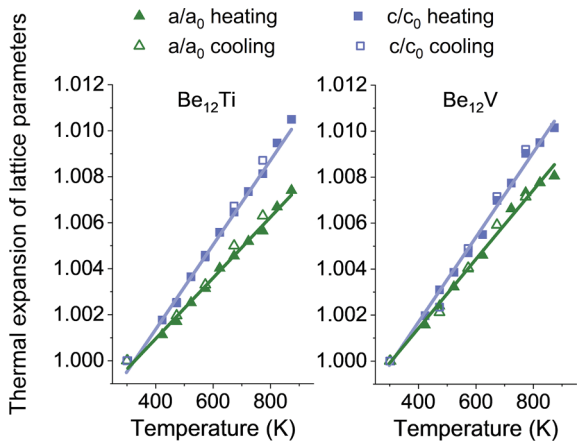

Fig. 4. Thermal expansion of lattice parameters (a/a_0 and c/c_0) of $Be_{12}Ti$ (left) and $Be_{12}V$ (right) where a_0 and c_0 are the lattice parameters at room temperature.

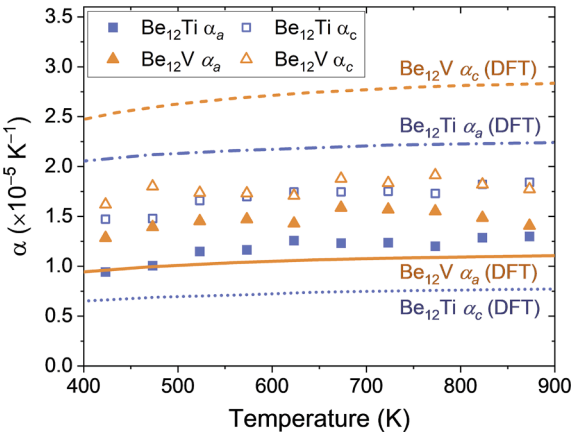

Fig. 5. Thermal expansion anisotropy in $Be_{12}Ti$ and $Be_{12}V$. The experimental thermal expansion coefficients obtained during heating in this work are compared with the calculation data using density functional theory (DFT) [11].

of goodness-of-fit [23]. R_{wp} is a discrepancy indicator, obtained by weighted sum of squared differences between experimental and computed intensities scaled by the weighted intensity. R_B is obtained from experimental and computed Bragg reflection intensities. S is defined as a ratio of R_{wp} to the minimum R_{wp} reachable, thus S becomes 1 in an ideal refinement. The profile fittings were considered satisfactory because the S factor was <1.3. Fig. 3 shows temperature dependencies of the lattice parameters and unit cell volumes using linear fitting. The results showed linear trend in the lattice parameters in this temperature range. Fig. 4 shows the thermal expansion along a- and c- axis, where a_0 and c_0 are the lattice parameters at RT. In the data collected while both heating and cooling, the gradient of c/c_0 was greater than that of a/a_0 for $Be_{12}Ti$ and $Be_{12}V$. It clearly indicates the anisotropic character of the thermal expansion in the beryllides, in which the tetragonal lattice preferentially expands along the c-axis direction. The direction of the thermal expansion anisotropy is contrary to the computational prediction for $Be_{12}Ti$, as shown in Fig. 5 and Table 2. The anisotropy was slightly greater for $Be_{12}Ti$ than that for $Be_{12}V$ (Fig. 4). The coefficients α_a and α_c at 873 K were 1.30 and 1.84 ($\times 10^{-5}$ K^{-1}) for $Be_{12}Ti$ and 1.40 and 1.77 ($\times 10^{-5}$ K^{-1}) for $Be_{12}V$. The ratios of α_a/α_c for $Be_{12}Ti$ and $Be_{12}V$ at 873 K were obtained to be 0.71 and 0.79, respectively. These values are comparable with the α_a/α_c ratio of hexagonal close-packed Be (0.8 at 873 K [20]). It is found that the anisotropy in thermal expansion is less significant than the computational prediction (α_a/α_c = 2.9 for $Be_{12}Ti$

Table 2
Thermal expansion coefficients along *a*- and *c*- axes (α_a and α_c), α_a/α_c, and volumetric thermal expansion coefficient α_V of $Be_{12}Ti$ and $Be_{12}V$ obtained during heating.

T (K)	$Be_{12}Ti$				$Be_{12}V$			
	α_a ($\times 10^{-5}$ K^{-1})	α_c ($\times 10^{-5}$ K^{-1})	α_V ($\times 10^{-5}$ K^{-1})	α_a/α_c	α_a ($\times 10^{-5}$ K^{-1})	α_c ($\times 10^{-5}$ K^{-1})	α_V ($\times 10^{-5}$ K^{-1})	α_a/α_c
423	0.94	1.47	1.06	0.64	1.28	1.62	1.35	0.79
473	1.01	1.48	1.12	0.68	1.39	1.80	1.48	0.77
523	1.15	1.66	1.27	0.69	1.45	1.74	1.51	0.84
573	1.16	1.70	1.30	0.69	1.47	1.73	1.52	0.85
623	1.26	1.75	1.38	0.72	1.43	1.71	1.49	0.84
673	1.23	1.75	1.36	0.71	1.59	1.88	1.64	0.84
723	1.24	1.75	1.37	0.71	1.57	1.84	1.62	0.86
773	1.20	1.73	1.34	0.69	1.55	1.91	1.63	0.81
823	1.29	1.82	1.43	0.71	1.49	1.82	1.56	0.82
873	1.30	1.84	1.44	0.71	1.41	1.77	1.49	0.79

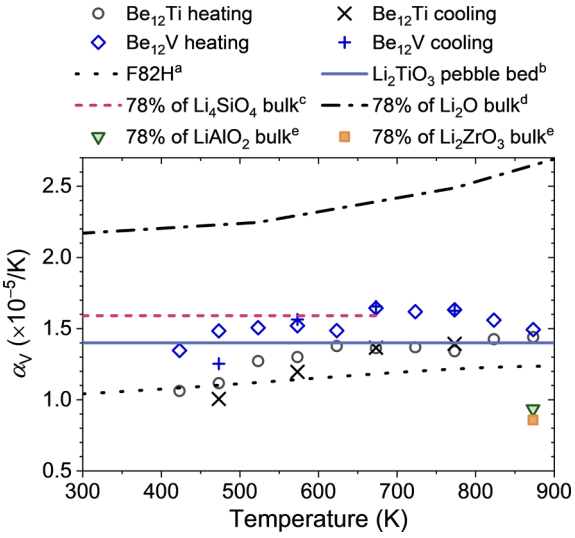

Fig. 6. Thermal expansion coefficient of $Be_{12}Ti$ and $Be_{12}V$ compared with those of F82H and Li_2TiO_3 pebble bed. The coefficients for Li_2O, Li_2ZrO_3, and $LiAlO_2$ pebble beds were estimated by multiplying the bulk values by 0.78. [a]Reference [28]. [b]Reference [24]. [c]Reference [25]. [d]Reference [27]. [e]Reference [26].

and $\alpha_a/\alpha_c = 0.4$ for $Be_{12}V$ at 873 K) [11].

The beryllide block will be directly contacted with either ceramic breeder pebbles or RAFM structural steel in the solid breeding blankets [17,18]. To assess the thermal compatibility, the average thermal expansion coefficients α_V were compared with those of the RAFM and ceramic breeder pebble bed, as shown in Fig. 6. The thermal expansion coefficient of Li_2TiO_3 pebble bed at RT to 973 K is reported to be $(1.4 \pm 0.2) \times 10^{-5}$ K^{-1} in the packing factor range of 65.3–68.3% [24]. It is reported that the thermal expansion coefficient of the pebble bed corresponds to 78% of the bulk material. Accordingly, the thermal expansion coefficients of the pebble bed for the ceramic breeder candidate materials (Li_2O, Li_4SiO_4, Li_2ZrO_3, and $LiAlO_2$)[25–27] were estimated by multiplying the bulk values by 0.78. The volumetric thermal expansion coefficients α_V (K^{-1}) of $Be_{12}Ti$ and $Be_{12}V$ at 873 K were given to be 1.46×10^{-5} and 1.51×10^{-5} K^{-1}, respectively. These values are in good agreement with the previous data by the thermo-mechanical analysis for $Be_{12}Ti$ and $Be_{12}V$ [21]. The thermal expansion coefficients of the bulk beryllides had a good agreement with those of the Li_2TiO_3 and Li_4SiO_4 pebble beds. The α_V values of the bulk beryllides also showed a good agreement with the empirical equation for the thermal expansion of the F82H steel [28]. In contrast, the estimated values for the Li_2O pebble bed were larger than the α_V of the beryllides, indicating a significant mismatch. The estimated coefficients for Li_2ZrO_3 and $LiAlO_2$ were estimated to be 8.6×10^{-6} and 9.4×10^{-6} K^{-1} at 873 K respectively, which were slightly lower than those for F82H and beryllides. This comparison indicates that $Be_{12}Ti$ and $Be_{12}V$ are highly compatible with the promising candidates of ceramic breeder materials and RAFM steel.

Conclusion

In this study, the thermal expansions of the advanced neutron multipliers, $Be_{12}Ti$ and $Be_{12}V$, were investigated using high-temperature X-ray diffraction (XRD) and subsequent Le Bail analysis with the partial structures. The results showed that the tetragonal unit cell of the beryllides expanded preferentially along the *c*-axis direction, with a moderately anisotropic characteristic comparable with that of hexagonal close-packed Be. The ratios of thermal expansion along *a*- and *c*-axes, α_a/α_c, for $Be_{12}Ti$ and $Be_{12}V$ were 0.71 and 0.79 at 873 K, respectively. In contrast, significant and opposite anisotropy computationally predicted for $Be_{12}Ti$ (i.e., $\alpha_a/\alpha_c \sim 2.5$ at 873 K) was not observed in this experiment. The volumetric thermal expansion coefficients of $Be_{12}Ti$ and $Be_{12}V$ at 873 K were 1.46×10^{-5} and 1.51×10^{-5} K^{-1}, respectively. The coefficients of the beryllides are in good agreement with those of F82H and pebble beds of Li_2TiO_3 and Li_4SiO_4, whereas a large mismatch is seen for Li_2O pebble bed.

CRediT authorship contribution statement

Keisuke Mukai: Conceptualization, Writing – original draft, Funding acquisition, Investigation, Data curation, Visualization. **Jae-Hwan Kim:** Methodology, Funding acquisition, Writing – review & editing. **Masaru Nakamichi:** Writing – review & editing, Supervision, Project administration.

Declaration of Competing Interest

The authors declare that they have no known competing financial interests or personal relationships that could have appeared to influence the work reported in this paper.

Data availability

Data will be made available on request.

Acknowledgement

This work was financially supported by a Grant-in-Aid for Scientific Research B (23H01156) from the Japan Society for the Promotion of Science (JSPS) and the Joint Usage/Research Program on Zero-Emission Energy Research, Institute of Advanced Energy, Kyoto University (ZE2021A-42, ZE2022A-36, ZE2023A-24).

References

[1] M. Nakamichi, J.H. Kim, Fabrication and hydrogen generation reaction with water vapor of prototypic pebbles of binary beryllides as advanced neutron multiplier,

Fusion Eng. Des. 98–99 (2015) 1838–1842, https://doi.org/10.1016/j.fusengdes.2015.04.026.
[2] M.M. Nakamura, J.H. Kim, M. Nakamichi, Y. Someya, K. Tobita, Y. Sakamoto, R. Hiwatari, Modeling of chemical reactions of beryllium/beryllide pebbles with steam for hydrogen safety design of water-cooled DEMO, Fusion Eng. Des. 136 (2018) 1484–1488, https://doi.org/10.1016/j.fusengdes.2018.05.039.
[3] J.H. Kim, M. Nakamichi, Characterization of modified $Be_{13}Zr$ beryllide pebbles as advanced neutron multipliers, Fusion Eng. Des. 146 (2019) 2608–2612, https://doi.org/10.1016/j.fusengdes.2019.04.054.
[4] Y. Fujii, M. Miyamoto, J.H. Kim, M. Nakamichi, N. Murayoshi, H. Iwakiri, Hydrogen retention behavior of beryllides as advanced neutron multipliers, Nucl. Mater. Energy. 9 (2016) 233–236, https://doi.org/10.1016/j.nme.2016.03.001.
[5] V. Chakin, R. Rolli, A. Moeslang, P. Kurinskiy, Tritium and helium release from highly neutron irradiated titanium beryllide, Fusion Eng. Des. 98–99 (2015) 1728–1732, https://doi.org/10.1016/j.fusengdes.2015.01.038.
[6] V. Chakin, R. Rolli, R. Gaisin, U. Hoeppener-Kramar, M. Nakamichi, M. Zmitko, Tritium release and retention in beryllium and titanium beryllide after neutron irradiation up to damage doses of 23–38 dpa, Fusion Eng. Des. 161 (2020), 111938, https://doi.org/10.1016/j.fusengdes.2020.111938.
[7] M. Miyamoto, Y. Sugimoto, D. Nishijima, M.J. Baldwin, R.P. Doerner, A. Zaloznik, J.H. Kim, M. Nakamichi, Comparative study of surface modification and D retention between beryllium and beryllides under high flux plasma exposure, Nucl. Mater. Energy. 27 (2021), 101014, https://doi.org/10.1016/j.nme.2021.101014.
[8] P.V. Vladimirov, V.P. Chakin, M. Dürrschnabel, R. Gaisin, A. Goraieb, F.A. H. Gonzalez, M. Klimenkov, M. Rieth, R. Rolli, N. Zimber, S. Udartsev, M. Kolmakov, A. Vechkutov, E. Frants, Development and characterization of advanced neutron multiplier materials, J. Nucl. Mater. 543 (2021), 152593, https://doi.org/10.1016/j.jnucmat.2020.152593.
[9] V. Chakin, A. Fedorov, R. Rolli, R. Gaisin, M. Klimenkov, J. Reimann, M. Nakamichi, Thermal conductivity of high-dose neutron irradiated beryllium and titanium beryllide, J. Nucl. Mater. 559 (2022), 153430, https://doi.org/10.1016/j.jnucmat.2021.153430.
[10] K. Mukai, R. Kasada, K. Yabuuchi, S. Konishi, J.-H. Kim, M. Nakamichi, Valence Electron and Chemical State Analysis of $Be_{12}M$ (M = Ti, V) Beryllides by Soft X-ray Emission Spectroscopy, ACS Appl. Energy Mater. 2 (2019) 2889–2895, https://doi.org/10.1021/acsaem.9b00223.
[11] B.L. Ji, C. Wang, S.X. Gu, Q. Qi, X.C. Li, H.S. Zhou, G.N. Luo, Comprehensive investigation of lattice dynamics of neutron multiplier beryllides: vibrational spectra and thermal performances, Nucl. Fusion. 63 (2023), https://doi.org/10.1088/1741-4326/aca8b9.
[12] D.V. Bachurin, P.V. Vladimirov, Ab initio study of Be and $Be_{12}Ti$ for fusion applications, Intermetallics. 100 (2018) 163–170, https://doi.org/10.1016/j.intermet.2018.06.009.
[13] Y. Wang, C. Wang, Z. Meng, J. Liu, Y. Li, L. Yang, Aggregation of retained helium and hydrogen in titanium beryllide Be12Ti: A first-principles study, RSC Adv. 11 (2021) 34860–34869, https://doi.org/10.1039/d1ra07023a.
[14] D.V. Bachurin, C. Stihl, P.V. Vladimirov, Ab initio study of hydrogen diffusion in Be and $Be_{12}Ti$ for fusion applications, Comput. Mater. Sci. 187 (2021), https://doi.org/10.1016/j.commatsci.2020.109921.
[15] M.L. Jackson, P.A. Burr, R.W. Grimes, Defect processes in $Be_{12}X$ (X = Ti, Mo, V, W), Nucl. Fusion. 57 (2017), 086049, https://doi.org/10.1088/1741-4326/aa7b41.
[16] K. Mukai, R. Kasada, J.H. Kim, M. Nakamichi, Electronic descriptors for vacancy formation and hydrogen solution in Be-rich intermetallics, Acta Mater. 241 (2022), 118428, https://doi.org/10.1016/j.actamat.2022.118428.
[17] Y. Someya, Y. Sakamoto, R. Hiwatari, Y. Miyoshi, S. Kakudate, H. Utoh, N. Asakura, Y. Homma, N. Nakajima, K. Tobita, Progress in Design and Engineering Issues on JA Demo, 28th IAEA Fusion Energy Conf. Nice, Fr. (2021) 10–15. https://nucleus.iaea.org/sites/fusionportal/Shared Documents/FEC 2020/fec2020-preprints/preprint0802.pdf.
[18] L.V. Boccaccini, F. Arbeiter, P. Arena, J. Aubert, L. Bühler, I. Cristescu, A. Del Nevo, M. Eboli, L. Forest, C. Harrington, F. Hernandez, R. Knitter, H. Neuberger, D. Rapisarda, P. Sardain, G.A. Spagnuolo, M. Utili, L. Vala, A. Venturini, P. Vladimirov, G. Zhou, Status of maturation of critical technologies and systems design: Breeding blanket, Fusion Eng. Des. 179 (2022), 113116, https://doi.org/10.1016/j.fusengdes.2022.113116.
[19] R. Gaisin, V. Chakin, P. Vladimirov, F.A. Hernández, S. Udartsev, A. Vechkutov, M. Kolmakov, Industrial-scale manufacturing experience of titanium beryllide block for DEMO blanket application, Fusion Eng. Des. 161 (2020), 111862, https://doi.org/10.1016/j.fusengdes.2020.111862.
[20] P. Gordon, A high temperature precision x-ray camera: Some measurements of the thermal coefficients of expansion of beryllium, J. Appl. Phys. 20 (1949) 908–917, https://doi.org/10.1063/1.1698252.
[21] J.H. Kim, M. Miyamoto, Y. Hujii, M. Nakamichi, Reactivity and deuterium retention properties of titanium-beryllium intermetallic compounds, Intermetallics. 82 (2017) 20–25, https://doi.org/10.1016/j.intermet.2016.11.005.
[22] F. Izumi, K. Momma, Three-dimensional visualization in powder diffraction, Solid State Phenom. 130 (2007) 15–20, https://doi.org/10.4028/www.scientific.net/SSP.130.15.
[23] R.A. Young, The Rietveld Method, Oxford University Press, 1993.
[24] H. Tanigawa, M. Enoeda, M. Akiba, Measurement of thermal expansion of Li2TiO3 pebble beds, Fusion Eng. Des. 82 (2007) 2259–2263, https://doi.org/10.1016/j.fusengdes.2007.06.023.
[25] N. Soga, Thermal Expansion Properties of Lithium Orthogermanate and Orthosilicate, J. Am. Ceram. Soc. 47 (1964) 469–469. https://doi.org/10.1111/j.1151-2916.1964.tb14441.x.
[26] W. Dienst, H. Zimmermann, Investigation of the mechanical properties of ceramic breeder materials, J. Nucl. Mater. 155–157 (1988) 476–479, https://doi.org/10.1016/0022-3115(88)90293-0.
[27] A. Donato, A critical review of Li2O ceramic breeder material properties correlations and data, Fusion Eng. Des. 38 (1998) 369–392, https://doi.org/10.1016/S0920-3796(97)00123-3.
[28] T. Hirose, T. Nozawa, R.E. Stoller, D. Hamaguchi, H. Sakasegawa, H. Tanigawa, H. Tanigawa, M. Enoeda, Y. Katoh, L.L. Snead, Physical properties of F82H for fusion blanket design, Fusion Eng. Des. 89 (2014) 1595–1599, https://doi.org/10.1016/j.fusengdes.2013.12.005.